Sciencexpress Report

Deterministic Generation of Single Photons from One Atom Trapped in a Cavity

J. McKeever, A. Boca, A. D. Boozer, R. Miller, J. R. Buck, A. Kuzmich, H. J. Kimble*

Norman Bridge Laboratory of Physics 12-33, California Institute of Technology, Pasadena, CA 91125, USA.

*To whom correspondence should be addressed. E-mail: hjkimble@caltech.edu

A single Cesium atom trapped within the mode of an optical cavity is used to generate single photons on demand. The photon wavepackets are emitted as a Gaussian beam with temporal profile and repetition rate controlled by external driving fields. Each generation attempt is inferred to succeed with probability near unity, while the efficiency for creating an unpolarized photon in the total cavity output is 0.69 ± 0.10, as limited by passive cavity losses. An average of 1.4 × 10⁴ photons are produced by each trapped atom. These results constitute an important step in quantum information science, for example toward the realization of distributed quantum networking.

A crucial building-block for quantum information science is a deterministic source of single photons that generates one-quantum wavepackets in a well controlled spatiotemporal mode of the electromagnetic field. For example, protocols for the implementation of quantum cryptography (*1*) and of distributed quantum networks rely on this capability (*2*), as do models for scalable quantum computation with single-photon pulses as flying qubits (*3–6*).

The earliest observations of single-photon emission used the fluorescent light from single atoms in two and three-level configurations (*7–9*), and thereby produced light with manifestly quantum or nonclassical character. Fluctuations in the number of atoms provided inherent limitations to these original schemes, and have since been mitigated by isolating single ions (*10*) and molecules (*11*, *12*), and by employing individual quantum dots (*13*, *14*) and color centers (*15*, *16*).

With a single dipole, pulsed excitation allows for ``triggered'' emission of a single photon within a prescribed interval, albeit into 4π steradians. To achieve emission as a directed output with high efficiency, the dipole emitter can be placed inside an optical resonator, as by coupling single quantum dots to microcavities (*17–19*). These experiments employ the Purcell effect to enhance radiative decay into a cavity mode of interest and thereby achieve a deterministic bit stream of single photon pulses (*20*) in a regime of weak coupling in cavity quantum electrodynamics (cQED).

By contrast, the generation of single photons within the domain of strong coupling in cQED (*21*, *22*) enables diverse new capabilities, including the reversible transfer of quantum states between atoms and photons as a fundamental primitive for the realization of quantum networks (*2*). A single photon source consisting of a trapped atom strongly coupled to an optical cavity represents an ideal node for such a network, in which long-lived internal atomic states can be mapped to quantum states of the electromagnetic field by way of "dark" eigenstates of the atom-cavity system (*23*). By way of a quantum repeater architecture, converting stationary qubits to flying qubits in this way enables distributed quantum entanglement over long distances (*2*).

We report on the deterministic generation of single-photon pulses by a single atom strongly coupled to an optical cavity in a configuration suitable for quantum network protocols. Single Cesium atoms are cooled and loaded into an optical trap (Fig. 1A) which localizes them within the mode of a high-finesse optical cavity (*24–26*). The atom is then illuminated by a sequence of laser pulses $\{\Omega_3^j(t),\Omega_4^j(t)\}$, the first of which $\Omega_3(t)$ drives a "dark-state" transfer between hyperfine ground states, $F = 3 \rightarrow 4$ (Fig. 1, B and C). In this process, one photon is created in the cavity mode because the atomic transition $F' = 3' \rightarrow F = 4$ is strongly coupled to the cavity field with rate g (*2*, *23*). The emitted photon leaves the cavity as a freely propagating, spatially Gaussian wavepacket whose temporal profile is determined by the external field $\Omega_3(t)$ (*2*, *20*, *23*). The atom is then recycled back to the original ground state by a second laser pulse $\Omega_4(t)$, and the protocol repeated for subsequent single photon generations.

The lifetime for a trapped atom in the presence of the driving $\Omega_{3,4}$ fields is $\tau_{trap} \cong 0.14$ s, which should be compared to the repetition period $\Delta t = 10$ μs for single-photon generation and to the lifetime of 3 s recorded in the absence of the $\Omega_{3,4}$ fields (*25*). Given our measured overall efficiency $\alpha = (2.4 \pm 0.4)\%$ for escape from the cavity, for propagation, and for photodetection (*26*), this means that on average, we generate (detect) about 1.4×10^4 (350) single photon pulses from each trapped atom.

The Gaussian beam emerging from the cavity mirror M_2 is directed to a beam splitter and then to two photon-counting detectors (D_A,D_B). For each atom k, photoelectric pulses from $D_{A,B}$ which occur during the trapping interval are stamped with their time of detection (with $\delta = 2$ ns time resolution) and recorded for later analysis. An example of the pulse shape for single photon generation is shown (Fig. 2A) over the detection window $[t_0^j, t_0^j+\delta t]$ within which the control field $\Omega_3^j(t)$ is ON, where $\delta t = 1$ μs, and t_0^j is the onset of $\Omega_3^j(t)$. The histogram of the total counts $n(t)$ from both detectors $D_{A,B}$, binned according to their delay with respect to t_0^j, is a sum over all repeated trials $\{j\}$ of the generation process from all atomic trapping events $\{k\}$. For the particular choice of $\Omega_3(t)$ employed here, single-photon pulses have duration $\tau \cong$ 120 ns (FWHM). The extended tail for $n(t)$ likely arises from generation attempts for which the atom resides in Zeeman sublevels that are weakly coupled to the control field at the beginning of the $\Omega_3(t)$ pulse (*27*, *28*), as well as from roughly two-fold variations in the coupling coefficient $g(\vec{r})$ (*29*). Qualitative agreement of this measured pulse shape has been obtained with multi-level quantum Monte Carlo simulations (*28*).

To investigate the quantum character of the emitted field, we calculate the function $C(\tau)$ obtained by cross-correlating the photoelectric counting events from the detectors $D_{A,B}$ as a function of time separation τ (Fig. 3) (*26*). The large suppression of $C(\tau)$ around $\tau = 0$ strongly supports the nonclassical character of the light pulses emitted by the atom-cavity system. The likelihood of two photons being detected within the same trial is greatly reduced relative to that for detection events in different trials.

Suppression of two-photon events is also quantified by the time dependence of the photon statistics over the course of the pulse (Fig. 2, B and C). Figure 2B displays the integrated probabilities for single $P_1(t)$ and joint $P_2(t)$ detection events for times t after the onset t_0^j of the control pulse $\Omega_3^j(t)$, with $P_2(t)$ normalized to $P_1(t)/2$. We calculate $P_1(t)$ and $P_2(t)$ for an effective single detector without dead time or after-pulsing, and define $P_{1,2} \equiv P_{1,2}(\delta t)$. Over the duration of the control pulse $0 \le t \le \delta t$, $P_1(t)$ rises to a final value $P_1 = 0.0284$; that is, the probability to register a single photoelectric event in a trial is 2.84%. The lower trace in Fig. 2B quantifies the suppression of joint detection events relative to that expected for a weak coherent state, which would have $2P_2(t)/P_1(t) \approx P_1(t)$ (as we have confirmed in separate measurements). By the end of the control pulse, $2P_2/P_1$ has reached the value 1.8×10^{-3}, which represents a 16-fold suppression of joint detection events relative to a Poisson process.

Figure 2C examines the ratio $R(t) \equiv [(P_1^2(t))/(2P_2(t))]$, where $R \approx 1$ for a weak coherent state and increases with suppression of two-photon events. Significantly, R is independent of propagation and detection losses for $P_1 >> P_2$. The trace in Fig. 2C restates the result that two-photon events are greatly suppressed relative to a coherent state, namely $R \equiv R(\delta t) = 15.9 \pm 1.0$. Also note that in Fig. 3, the average area of the large peaks in $C(\tau)$ around $\tau = j\Delta t$ should exceed that of the central peak around $\tau = 0$ by a factor of about R, which we have confirmed.

The background rate during the Ω_3 drive pulses is time-independent, and can be obtained from the record of photoelectric detections when no atom is trapped. The measured background count probability is $P_B = 2.7 \times 10^{-4}$ for the entire window, of which $P_D = 0.82P_B$ comes from detector dark counts, and the rest from various sources of scattered light. For an ideal single photon source, coincidence events at $D_{A,B}$ in the same trial would arise only because of background counts, since the source never emits two photons in one trial. Using the known values of $P_1(t)$ and P_B, the background-limited value $R_B(t)$ for this idealized scenario can be predicted. Our measured values are actually lower than this prediction ($R_B \equiv R_B(\delta t) = 52.5$), indicating a significant rate of excess coincidences.

These excess coincidences most likely arise from rare events with two atoms trapped within the cavity (*26*). We test this hypothesis in Fig. 4 by noting that the two-atom population should decay at roughly twice the rate of the single-atom population [as we have confirmed in other measurements related to Fig. 4 in (*25*)]. The probability P_2 for joint detection should therefore diminish as a function of duration of the trapping interval, with a corresponding increase in the ratio R, which is precisely the behavior evidenced in Fig. 4.

Operationally, we bin all our detection time-stamps according to their delay with respect to the trap-loading time ($t_T = 0$), and then compute photon statistics separately for each bin. Only 4 intervals in t_T are employed due to poor statistics for the coincidence counts, especially for large t_T. The analysis is the same as for Fig. 2, but we concentrate on the value $R \equiv R(\delta t)$, at the end of the $\Omega_3(t)$ pulse window. Furthermore, the ratio R_0 plotted in Fig. 4 is obtained from R with the contribution from the measured dark-count probability P_D removed, thereby providing a characterization of the atom-cavity source that is independent of the dark counts for our particular detectors. The results clearly support the hypothesis that rare two-atom events are responsible for our excess of coincidences.

Also shown in Fig. 4 as the full curve is the result for R_0 from a model calculation that assumes that a fraction η_I of our data is acquired with a single trapped atom, and that a fraction $\eta_{II} = 1-\eta_I$ has two atoms trapped, with η_I, η_{II} functions of the time t_T within the trapping interval (*26*). The correspondence between the model and our measurements supports the conclusion that excess coincidences arise from rare events with two atoms loaded into the trap. From this model, we infer that (i) approximately 3% of the trials are taken with two trapped atoms, and (ii) the generation of single photons succeeds with probability consistent with unity, $\phi_G = 1.15$

± 0.18 as constrained by our absolute knowledge of the various efficiencies (*26*).

Given our ability to distinguish multi-atom trap loading events in real time (as demonstrated in Fig. 4 of (*25*), events with $N \geq 2$ atoms trapped in the cavity could be actively discarded, or alternatively the extra atoms could be heated out of the trap, before even attempting single-photon generation. Moreover, in its current implementation, our atom-cavity system generates unpolarized single photons, with then a well defined polarization subsequently selected with 50% efficiency. This efficiency could be greatly improved by separating the functions of cooling and of single-photon generation for the Ω_3 control field, with the atom optically pumped into a known Zeeman sublevel before excitation. This separation of function would allow the interaction configuration of (*29*) to be implemented, making the pulse shape and phase for the photon wavepackets insensitive to randomness of the atomic position.

We have employed a single atom trapped within a high-finesse optical cavity as an efficient source for the generation of single photons on demand. The photons are emitted as a Gaussian beam with user-controlled pulse shapes. As documented in Fig. 4, the average ratio of single to two-photon event probabilities is $R_0 = 20.8 \pm 1.8$, while $R_0 \geq 150$ for single-photon generation at long trapping times $t_T \cong 0.4$ s. With this large suppression of two-photon probability, the Mandel-Q parameter is determined almost exclusively by propagation efficiency. For example, for polarized (unpolarized) photon wavepackets, $Q = -0.34 \pm 0.05$ ($Q = -0.68 \pm 0.10$) referenced to the total cavity output from (M_1,M_2). Absent passive losses from the cavity boundaries, the generation of single photons succeeds with probability close to unity, where this high success probability derives from the near ideal nature of the atom-cavity interaction in a regime of strong coupling.

References and Notes

1. N. Lutkenhaus, *Phys. Rev. A* **61**, 052304 (2000).
2. H.-J. Briegel, S. J. van Enk, J. I. Cirac, P. Zoller, in *The Physics of Quantum Information*, D. Bouwmeester, A. Ekert, A. Zeilinger, Eds. (Springer, Berlin, 2000), pp. 192-197.
3. I. L. Chuang, Y. Yamamoto, *Phys. Rev. A* **52**, 3489 (1995).
4. Q. A. Turchette, C. J. Hood, W. Lange, H. Mabuchi, H. J. Kimble, *Phys. Rev. Lett.* **75**, 4710 (1995).
5. E. Knill, R. Laflamme, G. Milburn, *Nature* **409**, 46 (2001).
6. L.-M. Duan, H. J. Kimble, in press (available at http://arXiv.org/abs/quant-ph/0309187).
7. J. F. Clauser, *Phys. Rev. D* **9**, 853 (1974).
8. H. J. Kimble, M. Dagenais, L. Mandel, *Phys. Rev. Lett.* **39**, 691 (1977).
9. P. Grangier, G. Roger, A. Aspect, *Europhys. Lett.* **1**, 173 (1986).
10. F. Diedrich, H. Walther, *Phys. Rev. Lett.* **58**, 203 (1987).
11. T. Basche, W. E. Moerner, M. Orrit, H. Talon, *Phys. Rev. Lett.* **69**, 1516 (1992).
12. B. Lounis, W. E. Moerner, *Nature* **407**, 491 (2000).
13. P. Michler *et al.*, *Nature* **406**, 968 (2000).
14. C. Santori, M. Pelton, G. Solomon, Y. Dale, Y. Yamamoto, *Phys. Rev. Lett.* **86**, 1502 (2001).
15. R. Brouri, A. Beveratos, J.-P. Poizat, P. Grangier, *Opt. Lett.* **25**, 1294 (2000).
16. C. Kurtsiefer, S. Mayer, P. Zarda, H. Weinfurter, *Phys. Rev. Lett.* **85**, 290 (2000).
17. P. Michler *et al.*, *Science* **290**, 2282 (2000).
18. E. Moreau *et al.*, *Appl. Phys. Lett.* **79**, 2865 (2001).
19. M. Pelton *et al.*, *Phys. Rev. Lett.* **89**, 233602 (2002).
20. C. K. Law, H. J. Kimble, *J. Mod. Opt.* **44**, 2067 (1997).
21. A. Kuhn, M. Hennrich, G. Rempe, *Phys. Rev. Lett.* **89**, 067901 (2002).
22. H. J. Kimble, *Phys. Rev. Lett.* **90**, 249801 (2003).
23. A. S. Parkins, P. Marte, and P. Zoller, H. J. Kimble, *Phys. Rev. Lett.* **71**, 3095 (1993).
24. J. Ye, D.W. Vernooy, H. J. Kimble, *Phys. Rev. Lett.* **83**, 4987 (1999).
25. J. McKeever *et al.*, *Phys. Rev. Lett.* **90**, 133602 (2003).
26. Materials and methods are available as supporting material on *Science* Online.
27. J. McKeever, A. Boca, A. D. Boozer, J. R. Buck, H. J. Kimble, *Nature* **425**, 268 (2003).
28. A. D. Boozer, A. Boca, J. R. Buck, J. McKeever, H. J. Kimble, in press (available at http://arXiv.org/abs/quant-ph/0309133).
29. L.-M. Duan, A. Kuzmich, H. J. Kimble, *Phys. Rev. A* **67**, 032305 (2003).

30. We gratefully acknowledge the contributions of K. M. Birnbaum, S. J. van Enk, H.-C. Nägerl, D. M. Stamper-Kurn, D. W. Vernooy, and J. Ye. This work was supported by the Caltech MURI Center for Quantum Networks under ARO Grant No. DAAD19-00-1-0374, by the National Science Foundation, and by the Office of Naval Research.

Supporting Online Material

www.sciencemag.org/cgi/content/full/1095232/DC1
Materials and Methods
Table S1
References

31 December 2003; accepted 18 February 2004
Published online 26 February 2004; 10.1126/science.1095232
Include this information when citing this paper.

Fig. 1. Illustration of the generation of single photons by one atom trapped in an optical cavity. (**A**) A single Cs atom is trapped in a cavity formed by the reflective surfaces of mirrors (M_1,M_2) and is pumped by the external fields (Ω_3,Ω_4)

(*25*). (**B**) The relevant atomic levels of the Cs D_2 line at 852.4 nm. Strong coupling at rate g is achieved for the transition $F^{\prime} = 3^{\prime} \rightarrow F = 4$ near a cavity resonance, where $g = 2\pi \times 16$ MHz. Atom and cavity decay rates $(\gamma,\kappa)/2\pi = (2.6$ MHz,4.2 MHz). (**C**) The timing sequence for the generation of successive single-photons by way of the $\Omega_{3,4}$ fields.

Fig. 2. (**A**) Total histogram of photoelectric detection events $n(t)$ from both detectors $D_{A,B}$. In all cases, the control field $\Omega_3(t)$ is initiated at time $t = 0$ with rise time 100 ns. (**B**) The integrated probability $P_1(t)$ for a single photoelectric event and ratio $2P_2(t)/P_1(t)$, where $P_2(t)$ is proportional to the integrated coincidence probability for joint detections from $D_{A,B}$. Note for a weak coherent state, the two traces would nearly overlap. (**C**) The ratio $R(t) = [(P_1^2(t))/(2P_2(t))]$ versus time, which indicates as high as 20-fold suppression of coincidences relative to a Poisson process.

Fig. 3. Time-resolved coincidences $C(\tau)$ as a function of delay τ between detections at $D_{A,B}$. Around $\tau = 0$, $C(\tau)$ is suppressed for two events from the same trial relative to its values for $\tau = j\Delta t$ for two events from different trials, where $j = \pm 1,2,\ldots$. As indicated in Fig. 1C, $\Delta t = 10$ μs is the repetition interval for the generation of single photons and $\delta t = 1$ μs is the duration of our control pulse Ω_3 (t).

Fig. 4. Evolution of the ratio $R_0 \equiv [(P_1^2)/(2P_2)]$ versus trapping time t_T, here corrected for detector dark counts. The data points are experimentally determined as discussed in the text, with vertical error bars based on counting statistics of coincidence events, and the horizontal bars indicating the bin widths in t_T. The full curve is the prediction from our model calculation that includes (rare) two-atom events. The dashed line represents the measured overall average of R_0 for all t_T.

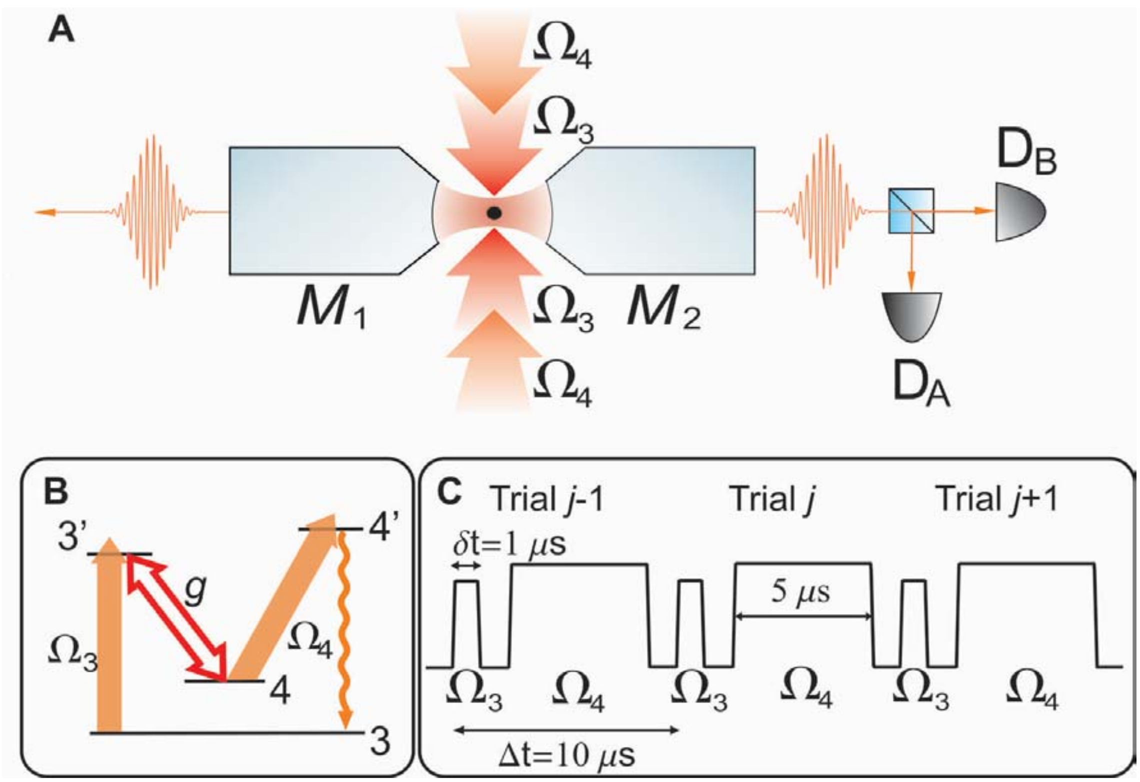

A
Ω4
Ω3
DB
M1
Ω3
M2
Ω4
DA
B
3'
g
4'
Ω3
Ω4
4
3
C
Trial j-1
Trial j
Trial j+1
δt=1 μs
5 μs
Ω3
Ω4
Ω3
Ω4
Ω3
Ω4
Δt=10 μs

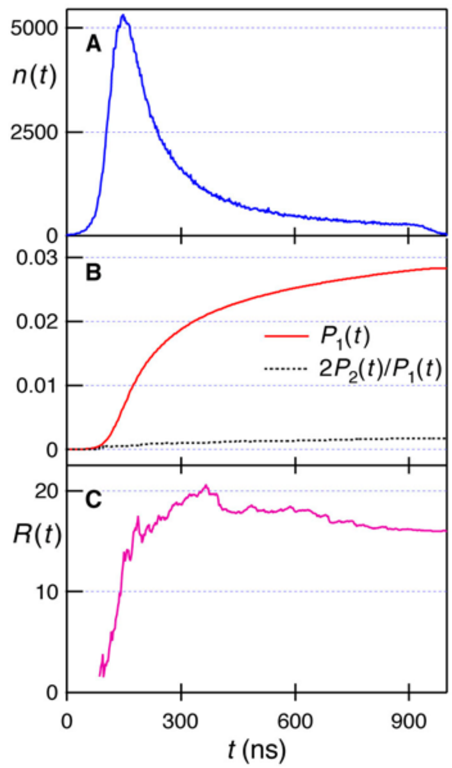

A
5000
2500
0
n(t)
B
0.03
0.02
0.01
0
P1(t)
2P2(t)/P1(t)
C
20
10
0
R(t)
0
300
600
900
t (ns)

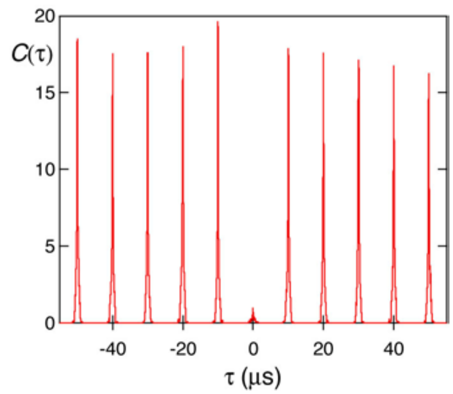
20
C(τ)
15
10
5
0
-40
-20
0
20
40
τ (μs)

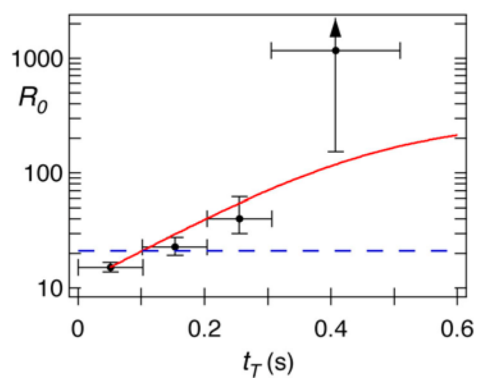

1000
R_0
100
10
0
0.2
0.4
0.6
t_T (s)